Homogenization of 3-D-Connected and Nonconnected Wire Metamaterials

Mário G. Silveirinha, *Member, IEEE,* and Carlos A. Fernandes, *Member, IEEE*

***Abstract*—The homogenization of composite structures made of long thin metallic wires is an important problem in electromagnetics because they are one of the basic components of the double-negative medium. In this paper, we propose a new analytical model to characterize the effective permittivity of the three-dimensional-wire medium in the long wavelength limit. We study two different topologies for the wire medium. The first structure consists of a lattice of connected wires, whereas the second one consists of a lattice in which the wires are not connected. Our results show that the propagation of electromagnetic waves in the two metamaterials is very different. While one of the structures exhibits strong spatial dispersion, the other one seems to be a good candidate for important metamaterial applications. We also found that, for extremely low frequencies, one of the structures supports modes with hyperbolic wave normal contours, originating negative refraction at an interface with air. We validated our theoretical results with numerical simulations.**

***Index Terms*—Double-negative (DNG) medium, homogenization theory, metamaterials, negative refraction, wire medium.**

I. Introduction

In [1], Smith *et al.* proposed an original structure that consists of a lattice of long metallic wires and split-ring resonators (SRRs). Theoretical and experimental studies show that the composite structure behaves as a double negative (DNG) medium (also known as left-handed medium) with a negative index of refraction [1]–[3]. This remarkable result motivated much research on metamaterials and potential applications. For example, numerous studies try to explore the focusing property of a DNG slab surrounded by conventional media [4]–[6]. It was even suggested, with considerable controversy, that metamaterials could be used to fabricate a super lens with no limit of resolution [6]. Other studies show that metamaterials may favor the miniaturization of some devices, and the realization of subwavelength cavity resonators [7].

The negative refraction of the DNG metamaterial is attributed to the combined effect of the arrays of wires and SRRs. As is well known, the lattice of wires is modeled as a medium with negative permittivity, whereas the lattice of SRRs is characterized by a negative permeability. To a first-order approximation, there is no coupling between the two basic inclusions.

Manuscript received May 20, 2004; revised September 20, 2004. This work was supported by the Fundação para Ciência e a Tecnologia under Project POSI 34860/99.

M. G. Silveirinha is with the Electrical Engineering Department–Instituto de Telecomunicações, Polo II da Universidade de Coimbra, 3030 Coimbra, Portugal (e-mail: mario.silveirinha@co.it.pt).

C. A. Fernandes is with the Instituto Superior Técnico–Instituto de Telecomunicações, Technical University of Lisbon, 1049-001 Lisbon, Portugal (e-mail: carlos.fernandes@lx.it.pt).

Digital Object Identifier 10.1109/TMTT.2005.845128

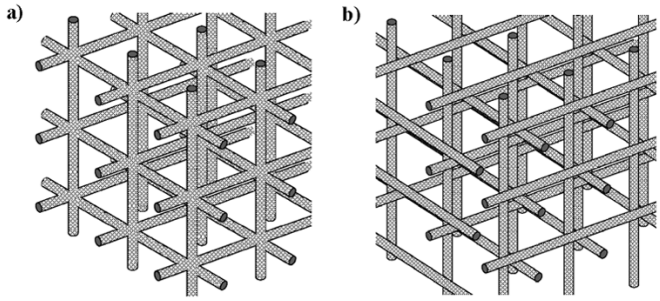

Fig. 1. (a) Fragment of a metamaterial formed by a lattice of connected wires. (b) Fragment of a metamaterial formed by a lattice of nonconnected wires (adjacent orthogonal wires are spaced of half-lattice constant).

The configuration originally proposed in [1] is characterized by DNG parameters only for a unique polarization, and for propagation along a specific direction of space. The fabrication of an isotropic DNG medium clearly compels for a basic cell with extra symmetry. Apparently, apart from practical difficulties related to technological limitations, the generalization seems to be straightforward.

However, the situation may not be so plain. For example, one might expect that a medium formed by wires that are parallel to the coordinate axes would interact with the radiation as an isotropic medium with negative permittivity. However, numerical results reported by Silveirinha and Fernandes [8] support that, at least for the nonconnected topology studied in [8], that is not the case. Indeed, we found that near the "plasma frequency" the referred metamaterial is not isotropic. Moreover, we verified that the numerical results are consistent with the hypothesis that, analogous with the one-dimensional (1-D)-wire medium formed by an array of parallel wires [9] and other related structures [10], the considered geometry for the three-dimensional (3-D)-wire medium has strong spatial dispersion in the long wavelength limit, i.e., the permittivity depends not only on the frequency, but also on the wave vector.

The results reported in [8] raise the obvious question: "Is it possible to fabricate an isotropic metamaterial with negative permittivity?" This is a fundamental subject not only to understand the possible limitations of DNG metamaterials, but also because metamaterials with negative permittivity, when paired with metamaterials with negative permeability, may have interesting properties and applications, as described in [11].

In this paper, we study two different topologies for the 3-D-wire medium. The first structure consists of a simple cubic lattice of connected wires, and the second one consists of a simple cubic lattice in which the wires are not connected (i.e., the geometry studied in [8] using numerical methods). In Fig. 1, we depict fragments of both metamaterials.

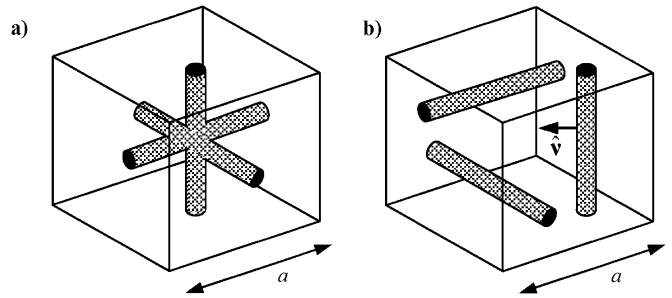

Fig. 2. Geometry of the unit cell. (a) Connected wire geometry. (b) Nonconnected wire geometry.

We propose a new analytical procedure to homogenize the periodic metamaterials. We will prove that the two topologies for the 3-D-wire medium are not equivalent, and that the interaction of electromagnetic waves with the two structures is very different. We will derive an approximate analytical formula for the effective permittivity of the composite structures. To our best knowledge, no results were reported in the literature that concern the homogenization of related structures with the exception of the numerical analysis described in [8], and the experimental results reported in [12] (the geometry considered in [12] is slightly more complex than the ones considered here).

This paper is organized as follows.[1] Sections II–IV concern the characterization of the Floquet modes that propagate in the periodic material. In Section II, we describe the geometry of the wire medium. In Section III, we formulate the modal problem, and we obtain the characteristic system using an integral-equation-based approach. In Section IV, we propose a simplified characteristic system that can be solved using analytical methods. Sections V and VI concern the homogenization of the metamaterials. In Section V, we explain how the effective permittivity dyadic can be obtained directly from the characteristic system. In Section VI, we discuss the physical phenomena implied by our formulas, and we compare the developed theory with full-wave numerical results. Finally, in Section VII, we present conclusions.

II. Geometry

We denote a generic point of space by $\mathbf{r} = (\mathbf{x}_1, \mathbf{x}_2, \mathbf{x}_3)$, and the unit vector directed along the x_n-direction by $\hat{\mathbf{u}}_n (n = 1, 2, 3)$. The wire medium is obtained by the periodic repetition of the unit cell Ω shown in Fig. 2. The unit cell is centered at the origin. The wires are arranged into a simple cubic lattice with lattice constant a. The boundary of the metallic region in the unit cell is denoted by ∂D, and the outward unit normal vector is denoted by $\hat{\mathbf{v}}$. For simplicity, we admit that the wires are embedded in air. We consider two different topologies for the wire medium. The geometry shown in Fig. 2(a) corresponds to the connected case, and the geometry of Fig. 2(b) corresponds to the nonconnected case. In Sections II-A and –B, we describe each configuration in detail.

[1]While this paper was being prepared, Simovski and Belov studied the homogenization of the nonconnected wire medium using a local field approach [23].

A. Connected Topology

In this case, the metallic region in the unit cell consists of three cylindrical wires with radius r_w and length a. We have

$$\partial D = \bigcup_{n=1}^{3} \partial D_n. \tag{1}$$

In the above, ∂D_n represents the surface of the wire section oriented along the x_n-direction. Note that the wires intersect mutually, forming a junction near the origin.

Our objective is to propose an analytical treatment for the homogenization problem. Thus, it is desirable to have a model as simple as possible for the current that flows along the wires. We will assume that $r_w \ll a \ll \lambda$, where λ is the wavelength of radiation in the dielectric region. Therefore, the thin-wire approximation can be used.

Within the thin-wire approximation, the density of current $\mathbf{J}_c$ over each wire flows along the direction of the axis, and has approximately circular symmetry. We will also admit that $\mathbf{J}_c$ is a traveling wave characterized by the wave vector $\mathbf{k} = (\mathbf{k}_1, \mathbf{k}_2, \mathbf{k}_3)$ (the justification for this assumption will be given in Section III). Therefore, we admit that

$$\mathbf{J}_c|_{\partial D_n} \approx \frac{I_n(x_n)}{2\pi r_w} e^{-j\mathbf{k}\cdot r} \hat{\mathbf{u}}_n, \qquad n = 1, \ldots, 3 \tag{2}$$

where I_n is a periodic function that stands for the unknown current. In order to take into account the coupling at the junction, we admit the possibility of the current induced over the nth wire being discontinuous at $x_n = 0$. In general, we have $[I_n] \equiv I_n(0^+) - I_n(0^-) \neq 0$. The conservation of current requires that (see also [13])

$$\sum_n [I_n] = 0. \tag{3}$$

Note that, within the described model, we completely neglect the shape of the wire junctions. Essentially, in our model, the junctions are replaced by infinitesimal gaps located at $x_n = 0, \pm a, \ldots$ (i.e., the points where we allow the current to be discontinuous) with a circular transverse section. Nevertheless, our simplified model is expected to yield good results since each junction occupies only a very small fraction of the unit cell.

B. Nonconnected Topology

The nonconnected geometry is depicted in Fig. 2(b). As in the previous case, the metallic region in the unit cell consists of three cylindrical wires with radius r_w and length a. Now the wires do not intersect, and the wire axes are spaced by $a/2$, i.e., a half-lattice constant. The wire oriented along the x_n-direction is centered at

$$\mathbf{r}_{0,n} = \frac{a}{4} \hat{\mathbf{u}}_n \times (\hat{\mathbf{u}}_1 + \hat{\mathbf{u}}_2 + \hat{\mathbf{u}}_3), \qquad n = 1, 2, 3. \tag{4}$$

As before, we admit that the density of current over the nth wire is given by (2). Now I_n is a continuous periodic function because there are no junctions.

III. Modal Problem

In order to homogenize the 3-D-wire medium, we will first characterize the Floquet modes propagating in the periodic metamaterial. Here, we will prove that the density of current associated with a generic electromagnetic mode satisfies a homogeneous characteristic system. Later we will show that the effective permittivity dyadic of the metamaterial can be obtained directly from the characteristic system.

By definition, an electromagnetic Floquet mode $(\mathbf{E},\mathbf{H})$ associated with the wave vector $\mathbf{k}=(\mathbf{k}_1,\mathbf{k}_2,\mathbf{k}_3)$ satisfies the following equations:

$$\nabla\times\mathbf{E}=-j\beta\eta\mathbf{H} \text{ dielectric region} \tag{5a}$$

$$\nabla\times\mathbf{H}=j\frac{\beta}{\eta}\mathbf{E} \text{ dielectric region} \tag{5b}$$

$$\hat{\mathbf{v}}\times\mathbf{E}=\mathbf{0} \text{ on the metallic surfaces} \tag{5c}$$

$$(\mathbf{E},\mathbf{H})\exp(j\mathbf{k}\cdot\mathbf{r}) \text{ is periodic} \tag{5d}$$

where η is the impedance of free space, $\beta=\omega/c$ is the free-space wavenumber, ω is the angular frequency, and c is the velocity of light in vacuum. In the above, (5a) and (5b) are the frequency-dependent Maxwell equations, (5c) is the boundary condition at the metallic interfaces, and (5d) is the Floquet wave condition.

As is well known, for each wave vector $\mathbf{k}$, the system of (5) represents an eigenvalue problem. It has nontrivial solutions only for a countable set of wavenumbers $\beta=\beta_n(\mathbf{k})$ $n=1,2,\ldots$. The eigenvalues $\beta=\beta_n(\mathbf{k})$ form the band structure of the periodic medium [14].

In what follows, we obtain an integral-equation-based formulation for the eigenvalue problem. To begin with, we note that an electromagnetic mode associated with the eigenvalue β and the wave vector $\mathbf{k}$ has the following integral representation:

$$\mathbf{E}(\mathbf{r})=\frac{\eta}{j\beta}\nabla\times\nabla\times\int_{\partial D}\mathbf{J}_c(\mathbf{r}')\mathbf{\Phi}_p(\mathbf{r}|\mathbf{r}')ds'. \tag{6}$$

In the above, the surface integral is over the primed coordinates (the integration is performed over the metallic surface in the unit cell), $\mathbf{r}$ is in the dielectric region, and $\mathbf{\Phi}_p=\mathbf{\Phi}_p(\mathbf{r}|\mathbf{r}';\beta,\mathbf{k})$ is the lattice Green function [15]–[17]. The lattice Green function is the Floquet solution of the following equation:

$$\nabla^2\mathbf{\Phi}_p+\beta^2\mathbf{\Phi}_p=-\sum_I\delta(\mathbf{r}-\mathbf{r}'-\mathbf{r}_I)e^{-j\mathbf{k}\cdot(\mathbf{r}-\mathbf{r}')} \tag{7}$$

where $\mathbf{I}=(\mathbf{i}_1,\mathbf{i}_2,\mathbf{i}_3)$ is a multiindex of integers, $\mathbf{r}=(\mathbf{x}_1,\mathbf{x}_2,\mathbf{x}_3)$ is the observation point, $\mathbf{r}'=(\mathbf{x}_1',\mathbf{x}_2',\mathbf{x}_3')$ is a source point, $\mathbf{r}_I=a\mathbf{I}$ is a lattice point, and δ is Dirac's distribution. We note that the Green function depends on both β and $\mathbf{k}$.

The lattice Green function can be efficiently evaluated as explained in [15]–[17]. Here, we instead consider the so-called spectral representation of the Green function, which is obtained by expanding $\mathbf{\Phi}_p$ into a Fourier series. The result is the following slowly convergent series:

$$\mathbf{\Phi}_p(\mathbf{r}|\mathbf{r}')=\frac{1}{V_{\text{cell}}}\sum_{\mathbf{J}}\frac{e^{-j\mathbf{k}_\mathbf{J}\cdot(\mathbf{r}-\mathbf{r}')}}{\mathbf{k}_\mathbf{J}\cdot\mathbf{k}_\mathbf{J}-\beta^2}$$
$$\mathbf{k}_\mathbf{J}=\mathbf{k}+\mathbf{k}_\mathbf{J}^0 \tag{8}$$

where $V_{\text{cell}}=a^3$ is the volume of the unit cell, $\mathbf{J}=(\mathbf{j}_1,\mathbf{j}_2,\mathbf{j}_3)$ is a multiindex of integers, and $\mathbf{k}_\mathbf{J}{}^0=(2\pi a)\mathbf{J}$. The spectral representation of the Green function has the important advantage that, due to its simplicity, many relevant integrals can be calculated in a closed analytical form.

It is clear that current density $\mathbf{J}_c=\hat{\mathbf{v}}\times\mathbf{H}$ is a Floquet wave associated with the same wave vector as the electromagnetic fields. This justifies our earlier assumption that $\mathbf{J}_c$ is a traveling wave [see (2)].

Now the idea is to obtain an integral equation for the current density. To this end, we impose that the tangential component of the electric field given by (6) is zero over the metallic surface. We test (6) with a generic tangential density $\mathbf{w}$, and then we integrate the resulting equation over ∂D. Using the standard method of moments (MoM) procedure, and also assuming that $\mathbf{w}$ is a traveling wave associated with the same wave vector as the electromagnetic mode, we are able to prove that

$$\chi(\mathbf{w},\mathbf{J}_c)=0 \tag{9}$$

where χ is the Hermitian form

$$\chi(\mathbf{w},\mathbf{J}_c)=\frac{1}{a^2}\int_{\partial D}\int_{\partial D}ds'ds\mathbf{\Phi}_p(\mathbf{r}|\mathbf{r}')\cdot(\nabla_S\cdot\mathbf{w}^*(\mathbf{r})\nabla_S'\cdot\mathbf{J}_c(\mathbf{r}')-\beta^2\mathbf{w}^*(\mathbf{r})\cdot\mathbf{J}_c(\mathbf{r}')). \tag{10}$$

In the above, the symbol * denotes the conjugate of a complex number, and ∇_S denotes the surface divergence. The previous result shows that for an electromagnetic mode associated with the eigenvalue β and the wave vector $\mathbf{k}$, the corresponding current density $\mathbf{J}_c$ is such that (9) holds for an arbitrary test density $\mathbf{w}$.

In analogy with (2), we assume in this paper that the test functions are of the form

$$\mathbf{w}|_{\partial D_m}=\frac{1}{2\pi r_w}w_m(x_m)e^{-j\mathbf{k}\cdot\mathbf{r}}\hat{\mathbf{u}}_m,\qquad m=1,2,3 \tag{11}$$

where w_m is a periodic function of x_m, possibly discontinuous at $x_m=0$, but such that $\sum_m[w_m]=0$, where $[w_m]\equiv w_m(0^+)-w_m(0^-)$. The expression for $\mathbf{w}$ is consistent with the thin-wire approximation described in Section II. The function w_m can be discontinuous only if the geometry of the wire medium corresponds to the connected case. It can be shown that the current conservation law $\sum_m[w_m]=0$ is a consequence of our simplified model for the wire junctions.

For a given wave vector $\mathbf{k}$, we can compute the eigenvalues $\beta_n=\beta_n(\mathbf{k})$ $n=1,2,\ldots$, using the standard approach described below. First, we expand $\mathbf{J}_c$ into a complete set of basis functions (with unknown coefficients), and substitute it in (9). We then test the resulting equation with a basis of test functions $\mathbf{w}$. In this way, we obtain a homogeneous linear system for the unknown coefficients. A nontrivial solution exists only if the determinant of the linear system vanishes. This occurs only if β is coincident with an eigenvalue.

We assume that the test functions are the same as the expansion functions. The test/expansion functions are denoted by $\mathbf{w}_q,\ q=1,2,\ldots$. The density of current is written as

$$\mathbf{J}_c = \sum_q c_q \mathbf{w}_q \tag{12}$$

where c_q are the unknown coefficients of the expansion.

Over the wire section ∂D_m, we assume that $\mathbf{w}_p$ evaluates to

$$\mathbf{w}_p|_{\partial D_m} = \frac{1}{2\pi r_w} w_{p,m}(x_m) e^{-j\mathbf{k}\cdot\mathbf{r}} \hat{\mathbf{u}}_m, \qquad m=1,2,3$$
$$\sum_m [w_{p,m}] = 0 \tag{13}$$

where, as in (11), $w_{p,m}(x_m)$ is a periodic function, possibly discontinuous at $x_m = 0$ (only if the wire medium is connected). The surface divergence of a generic test/expansion function satisfies

$$\nabla_S \cdot \mathbf{w}_p|_{\partial D_m} = \frac{1}{2\pi r_w}(\dot{w}_{p,m} - jk_m w_{p,m}) e^{-j\mathbf{k}\cdot\mathbf{r}}, \quad m=1,2,3. \tag{14}$$

In the above, $\dot{w}_{p,m}$ stands for the usual derivative of $w_{p,m}$ (i.e., the Dirac impulses that eventually arise must be discarded; indeed, the discontinuities are already taken into account by the current conservation law).

Using the approach delineated before, we obtain the homogeneous linear system

$$\lfloor \chi_{p,q} \rfloor \lfloor c_q \rfloor = 0 \quad \chi_{p,q} = \chi(\mathbf{w}_p, \mathbf{w}_q). \tag{15a}$$

We will refer to the above system as "the characteristic system." Straightforward calculations show that

$$\begin{aligned}\chi(\mathbf{w}_p,\mathbf{w}_q) = &\sum_{m,n} \frac{(k_m k_n - \beta^2 \delta_{m,n})}{a^2 (2\pi\, r_w)^2} \\ &\times \int_{\partial D_m} ds \int_{\partial D_n} ds' \mathbf{\Phi}_p(\mathbf{r}|\mathbf{r}') \\ &\cdot e^{j\mathbf{k}(\mathbf{r}-\mathbf{r}')} w^*_{p,m}(x_m) w_{q,n}(x'_n) \\ &+ \sum_{m,n} \frac{1}{a^2 (2\pi r_w)^2} \int_{\partial D_m} ds \int_{\partial D_n} ds' \mathbf{\Phi}_p(\mathbf{r}|\mathbf{r}') \\ &\cdot e^{j\mathbf{k}(\mathbf{r}-\mathbf{r}')} \dot{w}^*_{p,m}(x_m) \dot{w}_{q,n}(x'_n) \\ &+ \sum_{m,n} \frac{-jk_n}{a^2 (2\pi r_w)^2} \int_{\partial D_m} ds \int_{\partial D_n} ds' \mathbf{\Phi}_p(\mathbf{r}|\mathbf{r}') \\ &\cdot e^{j\mathbf{k}(\mathbf{r}-\mathbf{r}')} \dot{w}^*_{p,m}(x_m) w_{q,n}(x'_n) \\ &+ \sum_{m,n} \frac{jk_m}{a^2 (2\pi r_w)^2} \int_{\partial D_m} ds \int_{\partial D_n} ds' \mathbf{\Phi}_p(\mathbf{r}|\mathbf{r}') \\ &\cdot e^{j\mathbf{k}(\mathbf{r}-\mathbf{r}')} w^*_{p,m}(x_m) \dot{w}_{q,n}(x'_n). \end{aligned} \tag{15b}$$

For a given $\mathbf{k}$, the eigenvalues are the solutions of $\det(\lfloor \chi_{p,q} \rfloor) = 0$.

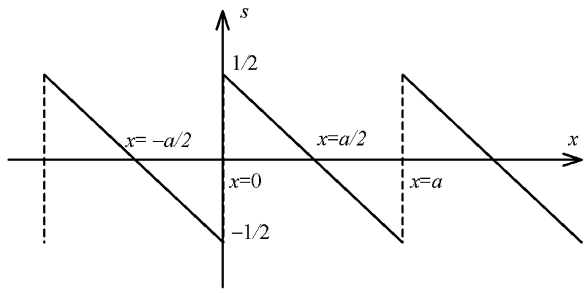

Fig. 3. "Saw" function.

IV. Long Wavelength Limit

Apart from the thin-wire approximation, the formulation presented in Section III is completely general. That formulation is mainly appropriate for the numerical calculation of the electromagnetic modes. However, numerical methods are computationally demanding and give no insight into the physics of the problem.

The objective here is to propose a simplified formulation that may allow characterizing the wire medium using analytical methods. The scope of application of our results is the long wavelength limit. The long wavelength limit approximation holds when

$$\beta a \ll 2\pi \text{ and } |\mathbf{k}| a \ll 2\pi. \tag{16}$$

The idea is to reduce the size of the characteristic system (which theoretically has infinite dimension) so that an analytical description is possible for the first few bands $\beta = \beta_n(\mathbf{k})$ of the periodic medium (i.e., for the eigenvalues with smaller amplitude). To begin with, it is appropriate to discuss some basic properties of the expansion functions.

A. Basis for the Test/Expansion Functions

Comparing (2) with (12), we see that the current over the wire oriented along the nth direction is given by

$$I_n(x'_n) = \sum_q c_q w_{q,n}(x'_n), \qquad n=1,2,3. \tag{17}$$

Since the I_n current is periodic, it seems appropriate to take the $w_{q,n}$ functions equal to the Fourier harmonics $\exp(jlx2\pi/a),\ l=0,\pm1,\ldots$ This set of expansion functions is clearly sufficient to model the electric current in the nonconnected topology case.

However, in the connected topology case, the set of Fourier harmonics is not enough to describe the electric current that flows along the wires (even though the Fourier basis is complete). In fact, the set of Fourier harmonics is continuous at $x'_n = 0$ and, thus, fails to model the possible discontinuous behavior of the current at the junctions (also note that the derivative of the current must be defined in the usual sense, and not in the distributional sense, as referred earlier). Hence, we need to incorporate some additional expansion functions in the expansion set.

The step discontinuity of the current can be cancelled out with another expansion function that has similar characteristics. This

extra expansion function may be rather arbitrary. For simplicity, we choose it to be the "saw" function $s(x)$, depicted in Fig. 3. For $0 < x < a$, the "saw" function is given by

$$s(x) = \frac{1}{2} - \frac{x}{a}, \qquad \text{for } 0 < x < a. \tag{18}$$

Obviously, the current I_n can be written as $I_n(x) = I_{c,n}(x) + [I_n]s(x)$, where $[I_n] \equiv I_n(0^+) - I_n(0^-)$ and $I_{c,n}$ is a continuous periodic function. Note that since $I_{c,n}$ is continuous, it can be expanded into a Fourier series with a good convergence rate. It is also important to remember that $[I_n]$ must follow the conservation law (3).

The previous discussion shows that, in the connected topology case, an appropriate basis for the test/expansion functions is formed by the two subsets described below. The first subset (subset I) is formed by the $\mathbf{w}_p$ vectors of type (13) such that the projection over a specific wire is a Fourier harmonic, and over the remaining wires is zero. The elements of this infinite set are continuous functions. Therefore, the conservation law $\sum_m [w_{p,m}] = 0$ is automatically observed.

The second subset (subset II) is formed by two elements only, and describes the discontinuous component of the currents. The elements of subset II are such that $w_{p,m}(x_m) = \alpha_{p,m}s(x_m)$, where $\alpha_{p,m}$ are constants, which ensure that the current conservation law $\sum_m \alpha_{p,m} = 0$ is satisfied (there exist precisely two independent vectors in such conditions). The eigenvalues of the propagation problem can be rigorously calculated (within the scope of our model) with the complete basis formed by subsets I and II.

In the nonconnected topology case, subset I is sufficient to characterize the wire medium, as explained earlier.

B. Simplified Characteristic System

The dimension of the characteristic system (15) is infinite. This seems to preclude the use of analytical techniques, as is our objective. However, in the long wavelength limit, the propagation in the wire medium can hopefully be described adequately using only the elements of the basis corresponding to the lowest order Fourier harmonics. Thus, we propose to truncate subset I, discarding all its elements, except the three vectors associated with the $l = 0$ Fourier harmonics $\exp(jlx_m 2\pi/a)$. We do not discard any element from subset II. Within this approximation, the dimension of linear system (15) is either drastically reduced to 3 in the nonconnected topology case or to $3 + 2 = 5$ in the connected topology case. This is equivalent to assume that, apart from the propagation factor, the amplitude of the current over each wire section is either constant (nonconnected topology) or a linear function (connected topology).

The elements of the truncated subset I are denoted by $\mathbf{w}_p^{\mathrm{I}}$ with $p = 1, 2, 3$, and are such that

$$w_{p,m}^{\mathrm{I}}(x_m) = \delta_{p,m}, \qquad p, m = 1, 2, 3. \tag{19}$$

On the other hand, the elements of subset II are denoted by $\mathbf{w}_p^{\mathrm{II}}$ with $p = 1, 2$ and, as explained above, they satisfy

$$w_{p,m}^{\mathrm{II}}(x_m) = \alpha_{p,m}s(x_m), \qquad m = 1, 2, 3; \quad p = 1, 2$$
$$\sum_m \alpha_{p,m} = 0. \tag{20}$$

For convenience, we introduce the following vectors:

$$\alpha_p = \sum_{1 \le m \le 3} \alpha_{p,m}\hat{\mathbf{u}}_m, \qquad p = 1, 2$$
$$\alpha_3 = \frac{1}{\sqrt{3}} \sum_{1 \le m \le 3} \hat{\mathbf{u}}_m. \tag{21}$$

We do not consider any specific choice for coefficients $\alpha_{p,m}$, $p = 1, 2$. We only assume that vectors α_1, α_2, and α_3 (defined as above) form an orthonormal basis of the space, and are real valued. Thus, we have

$$\alpha_p \cdot \alpha_q = \delta_{p,q}, \qquad p, q = 1, 2, 3. \tag{22}$$

Note that the orthogonality condition ensures that $\sum_m \alpha_{p,m} = 0$ is verified.

Within this approximation, we can rewrite the current expansion (12) as

$$\mathbf{J}_c = \sum_{1 \le q \le 3} I_{\mathrm{av},q}\mathbf{w}_q^{\mathrm{I}} + \sum_{1 \le q \le 2} c_q \mathbf{w}_q^{\mathrm{II}} \text{ (connected topology)} \tag{23a}$$

$$\mathbf{J}_c = \sum_{1 \le q \le 3} I_{\mathrm{av},q}\mathbf{w}_q^{\mathrm{I}} \text{ (nonconnected topology)} \tag{23b}$$

where the unknowns of the expansion are $I_{\mathrm{av},q}$ and c_q. We note that since the "saw" function is odd, we have

$$\frac{1}{a}\int_{\partial D} \mathbf{J}_c(\mathbf{r}')e^{j\mathbf{k}\cdot\mathbf{r}'}ds' = \sum_{1 \le q \le 3} I_{\mathrm{av},q}\hat{\mathbf{u}}_q. \tag{24}$$

Therefore, $I_{\mathrm{av},q}$ is the average current over the qth wire.

The characteristic system (15) is now rewritten using dyadic notation. In the connected topology case, we obtain

$$\begin{bmatrix} \overline{\overline{\mathbf{A}_{\mathrm{I}}}} & \overline{\overline{\mathbf{L}}} \\ \overline{\overline{\mathbf{L}^*}} & \overline{\overline{\mathbf{A}_{\mathrm{II}}}} \end{bmatrix} \begin{bmatrix} \mathbf{I}_{\mathrm{av}} \\ \mathbf{c} \end{bmatrix} = 0 \text{ (connected topology)} \tag{25a}$$

$$\overline{\overline{\mathbf{A}_{\mathrm{I}}}} = \sum_{p,q} \chi\left(\mathbf{w}_p^{\mathrm{I}}, \mathbf{w}_q^{\mathrm{I}}\right)\hat{\mathbf{u}}_p\hat{\mathbf{u}}_q, \qquad p, q = 1, 2, 3 \tag{25b}$$

$$\overline{\overline{\mathbf{A}_{\mathrm{II}}}} = \sum_{p,q} \chi\left(\mathbf{w}_p^{\mathrm{II}}, \mathbf{w}_q^{\mathrm{II}}\right)\hat{\mathbf{u}}_p\hat{\mathbf{u}}_q, \qquad p, q = 1, 2 \tag{25c}$$

$$\overline{\overline{\mathbf{L}}} = \sum_{p,q} \chi\left(\mathbf{w}_p^{\mathrm{I}}, \mathbf{w}_q^{\mathrm{II}}\right)\hat{\mathbf{u}}_p\hat{\mathbf{u}}_q, \qquad p = 1, 2, 3; \quad q = 1, 2. \tag{25d}$$

In the above, $\overline{\overline{\mathbf{L}^*}}$ denotes the conjugate of the transpose of the dyadic $\overline{\overline{\mathbf{L}}}$, χ denotes the form (10), and $\mathbf{c} = \sum_q c_q\hat{\mathbf{u}}_q$ and $\mathbf{I}_{\mathrm{av}} = \sum_{1 \le q \le 3} I_{\mathrm{av},q}\hat{\mathbf{u}}_q$ denote the vectors that represent the unknowns.

Similarly, in the nonconnected topology case, the characteristic system becomes $\overline{\overline{\mathbf{A}_{\mathrm{I}}}} \cdot \mathbf{I}_{\mathrm{av}} = 0$. Note that the dyadic $\overline{\overline{\mathbf{A}_{\mathrm{I}}}}$ depends on the specific topology of the wire medium. Indeed, in the connected case, the wires in the unit cell are centered at the origin, whereas in the nonconnected case, they are not and, thus, $\chi\left(\mathbf{w}_p^{\mathrm{I}}, \mathbf{w}_q^{\mathrm{I}}\right)$ will be different in the two situations.

It is convenient to rewrite the characteristic system in a unified manner. As proven in Appendix A, the dyadic $\overline{\overline{\mathbf{A}_{\mathrm{II}}}}$ is invertible. Therefore, we can calculate vector $\mathbf{c}$ as a function of $\mathbf{I}_{\mathrm{av}}$ and considerably simplify (25). After straightforward calculations, we find that

$$\overline{\overline{\mathbf{A}}} \cdot \mathbf{I}_{\mathrm{av}} = 0$$

where

$$\overline{\overline{\mathbf{A}}} = \begin{cases} \overline{\overline{\mathbf{A}_{\mathrm{I}}}} - \overline{\overline{\mathbf{L}}} \cdot \overline{\overline{\mathbf{A}_{\mathrm{II}}}}^{-1} \cdot \overline{\overline{\mathbf{L}^*}} \text{ connected topology} \\ \overline{\overline{\mathbf{A}_I}} \text{ nonconnected topology.} \end{cases} \tag{26}$$

For a given $\mathbf{k}$, the eigenvalues associated with the first few modes can be obtained by solving the characteristic equation $\det(\overline{\overline{\mathbf{A}}}) = 0$ for β.

C. Dyadic $\overline{\overline{\mathbf{A}}}$

In order to keep the readability of this paper, the calculation of the dyadic $\overline{\overline{\mathbf{A}}}$ is addressed in Appendix A. In the long-wavelength limit, we obtain

$$\overline{\overline{\mathbf{A}}} = \overline{\overline{\mathbf{A}_0}} + \overline{\overline{\mathbf{A}_{\mathrm{reg}}}} \tag{27a}$$

$$\overline{\overline{\mathbf{A}_0}} = \frac{1}{V_{\mathrm{cell}}} \frac{1}{k^2 - \beta^2} \left(\mathbf{kk} - \beta^2 \overline{\overline{\mathbf{I}}} \right) \tag{27b}$$

$$\overline{\overline{\mathbf{A}_{\mathrm{reg}}}} = \begin{cases} \dfrac{1}{V_{\mathrm{cell}}} \dfrac{1}{3} \left(\dfrac{1}{\beta_0^2} + \dfrac{2}{\beta_1^2} \right) \mathbf{kk} - \dfrac{1}{V_{\mathrm{cell}}} \dfrac{\beta^2}{\beta_0^2} \overline{\overline{\mathbf{I}}} \text{ (connect. } t.) \\ \dfrac{1}{V_{\mathrm{cell}}} \dfrac{1}{\beta_0^2} \sum\limits_m \left(k_m^2 - \beta^2 \right) \hat{\mathbf{u}}_m \hat{\mathbf{u}}_m \text{ (nonconnect. } t.) \end{cases} \tag{27c}$$

where $\overline{\overline{\mathbf{I}}} = \sum_{1 \le m \le 3} \hat{\mathbf{u}}_m \hat{\mathbf{u}}_m$ is the identity dyadic, $k_m = \mathbf{k} \cdot \hat{\mathbf{u}}_m$, and $k^2 = \overline{\mathbf{k}} \cdot \overline{\mathbf{k}}$. Constants β_0 and β_1 are defined by (B5) and (B6), and depend exclusively on the wire radius and lattice constant.

For future reference, we note that the inverse dyadics are given by

$$\overline{\overline{\mathbf{A}_0}}^{-1} = \frac{V_{\mathrm{cell}}}{\beta^2} \left((\beta^2 - k^2) \overline{\overline{\mathbf{I}}} + \mathbf{kk} \right) \tag{28}$$

$$\overline{\overline{\mathbf{A}_{\mathrm{reg}}}}^{-1} = V_{\mathrm{cell}} \left(-\frac{\beta_0^2}{\beta^2} \right) \left(\overline{\overline{\mathbf{I}}} - \frac{\mathbf{kk}}{k^2 - l_0 \beta^2} \right)$$

$$l_0 = \frac{3}{1 + 2\dfrac{\beta_0^2}{\beta_1^2}} \text{ (connected topology)} \tag{29a}$$

$$\overline{\overline{\mathbf{A}_{\mathrm{reg}}}}^{-1} = V_{\mathrm{cell}} \sum_m \frac{\beta_0^2}{(\beta^2 - k_m^2)} \hat{\mathbf{u}}_m \hat{\mathbf{u}}_m \text{ (nonconnected top).} \tag{29b}$$

V. Homogenization of the Wire Medium

Here, we will explain how the effective permittivity of the wire medium can be directly obtained from the characteristic system derived in Section IV. To begin, it is appropriate to introduce some auxiliary results and definitions that will be important later.

A. Homogenization Basics

Let $(\mathbf{E}, \mathbf{B})$ be an electromagnetic Floquet mode in a generic metallic crystal, i.e., a solution of (5) with $\mathbf{H} = \mathbf{B}/\mu_0$, where $\mathbf{B}$ is the magnetic induction. We define the average fields $\mathbf{E}_{\mathrm{av}}$ and $\mathbf{B}_{\mathrm{av}}$ as follows:

$$\mathbf{E}_{\mathrm{av}} = \frac{1}{V_{\mathrm{cell}}} \int_\Omega \mathbf{E}(\mathbf{r}) e^{+j\mathbf{k}\cdot\mathbf{r}} d^3\mathbf{r}$$
$$\mathbf{B}_{\mathrm{av}} = \frac{1}{V_{\mathrm{cell}}} \int_\Omega \mathbf{B}(\mathbf{r}) e^{+j\mathbf{k}\cdot\mathbf{r}} d^3\mathbf{r}. \tag{30}$$

Using (5), it can be verified that the following equations hold:

$$-\mathbf{k} \times \mathbf{E}_{\mathrm{av}} + \beta\eta \frac{\mathbf{B}_{\mathrm{av}}}{\mu_0} = 0 \tag{31a}$$

$$\beta \mathbf{E}_{\mathrm{av}} + \mathbf{k} \times \eta \frac{\mathbf{B}_{\mathrm{av}}}{\mu_0} = \frac{j\eta}{V_{\mathrm{cell}}} \int_{\partial D} \mathbf{J}_c e^{+j\mathbf{k}\cdot\mathbf{r}} ds \tag{31b}$$

where ∂D denotes the surface of the metallic region in the unit cell and $\mathbf{J}_c = \hat{\mathbf{v}} \times \mathbf{B}/\mu_0$ is the surface current over the metallic interfaces. Using (31) and (24), after straightforward manipulations, we obtain

$$\frac{-1}{\beta^2} \left((\beta^2 - k^2) \overline{\overline{\mathbf{I}}} + \mathbf{kk} \right) \cdot \mathbf{E}_{\mathrm{av}} = \frac{\eta}{j\beta V_{\mathrm{cell}}} \int_{\partial D} \mathbf{J}_c e^{+j\mathbf{k}\cdot\mathbf{r}} ds = \frac{\eta}{j\beta a^2} \mathbf{I}_{\mathrm{av}}. \tag{32}$$

Provided that magnetization and higher dipole moments can be neglected, the right-hand side of the above equation is approximately equal to $\mathbf{P}/\varepsilon_0$, where $\mathbf{P}$ is the polarization vector (i.e., the spatial average electric dipole moment in a unit cell). That is the case in this paper because, at least within the scope of our thin-wire model, the magnetization is exactly zero.

For future reference, we note that (32) can be rewritten as

$$\overline{\overline{\mathbf{A}_0}}^{-1} \cdot \mathbf{E}_{\mathrm{av}} = -\frac{V_{\mathrm{cell}} \eta}{j\beta a^2} \mathbf{I}_{\mathrm{av}} \tag{33}$$

where $\overline{\overline{\mathbf{A}_0}}^{-1}$ is defined by (28).

B. Effective Permittivity Dyadic

Here, we prove that the effective medium can be characterized with a permittivity dyadic. From (26) and (33), we have

$$\overline{\overline{\mathbf{A}}} \cdot \overline{\overline{\mathbf{A}_0}}^{-1} \cdot \mathbf{E}_{\mathrm{av}} = 0. \tag{34}$$

We claim that the characteristic system $\det(\overline{\overline{\mathbf{A}}}) = 0$ is equivalent to the characteristic system $\det(\overline{\overline{\mathbf{A}}} \cdot \overline{\overline{\mathbf{A}_0}}^{-1}) = 0$ (i.e., both systems yield the same eigenvalues β for the propagation problem). Indeed, although $\det(\overline{\overline{\mathbf{A}_0}}^{-1}) = 0$ for $\beta^2 = k^2$, we have $\det(\overline{\overline{\mathbf{A}}} \cdot \overline{\overline{\mathbf{A}_0}}^{-1}) \neq 0$ for $\beta^2 = k^2$ because $\det(\overline{\overline{\mathbf{A}}})$ has a pole and there is the following pole-zero cancellation:

$$\overline{\overline{\mathbf{A}}} \cdot \overline{\overline{\mathbf{A}_0}}^{-1} = (\overline{\overline{\mathbf{A}_0}} + \overline{\overline{\mathbf{A}_{\mathrm{reg}}}}) \cdot \overline{\overline{\mathbf{A}_0}}^{-1} = \overline{\overline{\mathbf{I}}} + \overline{\overline{\mathbf{A}_{\mathrm{reg}}}} \cdot \overline{\overline{\mathbf{A}_0}}^{-1}. \tag{35}$$

Next, we obtain an explicit formula for the effective permittivity of the metamaterial. Inserting (35) into (34), after simple manipulations, we obtain

$$\left(\overline{\overline{\mathbf{A}_{\mathrm{reg}}}}^{-1} + \overline{\overline{\mathbf{A}_0}}^{-1} \right) \cdot \mathbf{E}_{\mathrm{av}} = 0. \tag{36}$$

Using (28), the above formula can be rewritten as follows:

$$\left(\mathbf{kk} - k^2\bar{\bar{\mathbf{I}}} + \beta^2\bar{\bar{\varepsilon}}\right)\cdot\mathbf{E}_{\rm av} = 0$$

where

$$\bar{\bar{\varepsilon}} = \bar{\bar{\mathbf{I}}} + \frac{1}{V_{\rm cell}}\overline{\overline{\mathbf{A}_{\rm reg}}}^{-1}. \tag{37}$$

Comparing the above expression with the characteristic equation for the average electric field in an anisotropic medium [18, p. 202], we recognize that $\bar{\bar{\varepsilon}}$ is necessarily the (relative) effective permittivity dyadic. Indeed, from (32) and (37) (and noting, as before, that the right-hand side of (32) is $\mathbf{P}/\varepsilon_0$), we have

$$\frac{\mathbf{P}}{\varepsilon_0} = (\bar{\bar{\varepsilon}} - \bar{\bar{\mathbf{I}}})\cdot\mathbf{E}_{\rm av}. \tag{38}$$

From (29), the effective permittivity of the wire medium is given by

$$\bar{\bar{\varepsilon}} = \bar{\bar{\mathbf{I}}} - \frac{\beta_0^2}{\beta^2}\left(\bar{\bar{\mathbf{I}}} - \frac{\mathbf{kk}}{k^2 - l_0\beta^2}\right)$$

$$l_0 = \frac{3}{1 + (3-1)\dfrac{\beta_0^2}{\beta_1^2}} \text{ (connected topology)} \tag{39a}$$

$$\bar{\bar{\varepsilon}} = \bar{\bar{\mathbf{I}}} - \sum_{1\le m\le 3}\frac{\beta_0^2}{(\beta^2 - k_m^2)}\hat{\mathbf{u}}_m\hat{\mathbf{u}}_m \text{ (nonconnected topology)}. \tag{39b}$$

Note that the effective permittivity depends explicitly on the wave vector and, thus, the wire medium suffers from spatial dispersion.

We could homogenize the 1-D-wire medium (array of parallel wires) and the two-dimensional (2-D)-wire medium (two arrays of orthogonal wires) using exactly the same technique (see Appendix C). For the 1-D-wire medium case, we would find that the permittivity dyadic is given by (39b) with the m index restricted to $m = 3$ (assuming that the wires are oriented along the x_3-direction). Comparing that formula with the results described in [9], we conclude that the constant β_0 must be equal to $\beta_0 = \omega_0/c$, where ω_0 is the plasma (angular) frequency, and c is the velocity of light in vacuum. Indeed, numerical simulations and analytical results show that, to a good approximation, β_0 given by (B5) is coincident with the result of [9]

$$(\beta_0 a)^2 \approx \frac{2\pi}{\ln\left(\dfrac{a}{2\pi r_w}\right) + 0.5275}. \tag{40}$$

The above formula can be used to compute β_0 quickly and with good accuracy. On the other hand, (B5) is a slowly convergent double series and, thus, numerous terms need to be summed.

To conclude, we note that the homogenization method described here can be generalized to arbitrary periodic structures, and used to extract the permittivity, permeability, and magnetoelectric terms of the effective medium.

VI. Discussion

Here, we will characterize the electromagnetic modes that can propagate in the homogenized medium, and discuss the physical implications of the results. We also compare our analytical model with full-wave numerical simulations.

To begin with, we note that, from (37), the dispersion characteristic of the modes can be calculated by solving the characteristic equation

$$\det\left(\mathbf{kk} - k^2\bar{\bar{\mathbf{I}}} + \beta^2\bar{\bar{\varepsilon}}\right) = 0. \tag{41}$$

The solutions of the characteristic equation depend on the topology of the wire medium, and are described in Sections VI-A and B.

A. Connected Geometry

Here, we admit that the wires are connected and, thus, the permittivity dyadic is given by (39a). This model for the permittivity is exactly coincident with the one described in [19] for the effective permittivity of a nonmagnetized plasma considering the effect of pressure forces. Unlike the classic "cold" plasma model [19], which applies when the pressure forces are neglected, this model is characterized by spatial dispersion in the long wavelength limit. A "cold" plasma is characterized by the permittivity $\varepsilon_{\rm TEM} = \left(1 - \beta_0^2/\beta^2\right)$.

It is easy to verify that (39a) predicts that there are two degenerate TEM modes (i.e., such that $\mathbf{k}\cdot\mathbf{E}_{\rm av} = 0$) with the dispersion characteristic

$$\beta^2 = \beta_0^2 + k^2 \text{ (TEM modes)}. \tag{42}$$

Since $\bar{\bar{\varepsilon}}\cdot\mathbf{E}_{\rm av} = (1 - \beta_0^2/\beta^2)\mathbf{E}_{\rm av}$ when $\mathbf{k}\cdot\mathbf{E}_{\rm av} = 0$, we conclude that the TEM waves "see" the effective permittivity $\varepsilon_{\rm TEM}$. Therefore, in the long wavelength limit, TEM propagation in the 3-D-wire medium is equivalent to propagation in "cold" plasma.

Apart from the TEM waves discussed above, the 3-D-wire medium supports a longitudinal wave. The longitudinal wave is such that the polarization is parallel to the wave vector. It starts propagating near the plasma frequency and has the dispersion characteristic

$$\beta^2 = \beta_0^2 + \frac{1}{l_0}k^2,$$
$$\frac{1}{l_0} = \frac{1}{3}\left(1 + 2\frac{\beta_0^2}{\beta_1^2}\right) \text{ (longitudinal mode)}. \tag{43}$$

The "cold" plasma model also predicts a similar mode [19]. However, since the "cold" plasma model neglects the "pressure forces," the corresponding mode is dispersionless, i.e., $\beta^2 = \beta_0^2$. If the "pressure forces" are considered, the electrodynamics is exactly the same as in the wire medium. The existence of a longitudinal mode was also conjectured in [12] based on experimental results.

Next, we present full-wave numerical simulations that validate the above-described results. We numerically implemented the full-wave method described in [8] also using the thin-wire approximation. We expanded the unknown currents with $5 +$

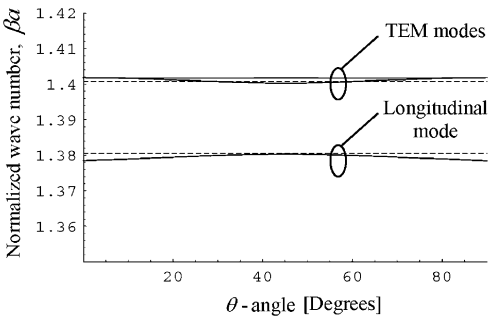

Fig. 4. Dispersion characteristic of the modes as a function of the θ angle for $\varphi = 0°$ (full line: numerical results; dashed line: theory).

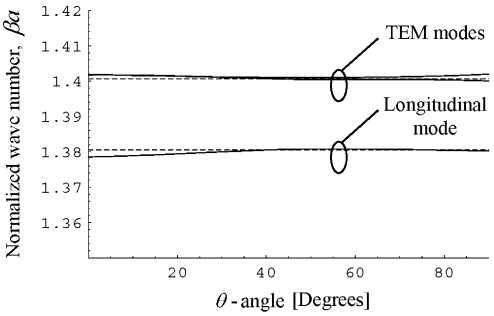

Fig. 5. Dispersion characteristic of the modes as a function of the θ angle for $\varphi = 45°$ (full line: numerical results; dashed line: theory).

$5 + 5 + 2 = 17$ expansion functions (the continuous component of each current was expanded with five Fourier harmonics; the coupling between the wires is modeled with two expansion functions; the expansion basis for the currents is the same as the one discussed in Section IV).

We admit that $r_w = 0.01a$ and, thus, the plasma wavenumber is $\beta_0 a \approx 1.37$ and $\beta_1 a \approx 3.55$. We put $\mathbf{k} = k(\cos\varphi \sin\theta, \sin\varphi \sin\theta, \cos\theta)$ with $k = 0.1\pi/a$, and we computed β numerically for the relevant modes as a function of θ for $\varphi = 0°$ (Fig. 4) and $\varphi = 45°$ (Fig. 5).

As can be seen in Figs. 4 and 5, the agreement between the full-wave results and the analytical model is good.

The results show that the connected medium is a good candidate to synthesize a metamaterial with negative permittivity, at least if the longitudinal mode is not significantly excited. To study this subject with greater detail, one would need to know the boundary conditions for the electromagnetic fields at an interface with a dielectric. As is well known, the usual boundary conditions (i.e., the continuity of the tangential components) are insufficient to describe the reflection of plane waves at an interface. Indeed, we need an additional boundary condition [20], [21] as a consequence of the medium response being spatially nonlocal (i.e., the electric displacement at one point depends on the electric field in the whole material). Unfortunately, no general method to obtain the additional boundary conditions is available [20]. A detailed discussion of this topic is outside the scope of this paper.

We will instead discuss the use of the connected geometry of the wire medium in DNG material applications. Let us suppose that an ideal isotropic magnetic particle is available (e.g., a generalization of the split ring resonator [22]). If we load the wire medium with magnetic particles, it seems reasonable to assume (provided there is low interaction between the wires and magnetic particle) that the new composite medium is described by the permittivity dyadic (39a) and a permeability μ due to the magnetic effects. We assume that μ is a scalar and that $\mu < 0$ in some frequency band below the plasma frequency. We claim that this new composite material behaves as an ideal isotropic DNG material in the referred frequency band and that no spatial dispersion occurs in this band. Indeed, it is easy to verify that only two TEM modes will propagate in this regime. The longitudinal mode of the wire medium will remain in cutoff even though $\mu < 0$. The reason is very simple: the magnetic field associated with the longitudinal mode is exactly zero and, thus, this mode does not interact with the magnetic particles. Thus, we conclude that this topology of the wire medium may be adequate for DNG material applications.

B. Nonconnected Geometry

Here, we consider that the wires are not connected. Unlike the previous case, the dispersion characteristic and polarization vector cannot be calculated in closed analytical form. To circumvent this problem, we proceed as follows. First, we write the wave vector in polar coordinates, i.e., $\mathbf{k} = k(\sin\theta\cos\varphi, \sin\theta\sin\varphi, \cos\theta)$. We then admit that the dispersion characteristic has the Taylor expansion $\beta^2 = a_0 + a_2 k^2 + \cdots$, where a_0, a_2, etc. are unknown coefficients that, in general, depend on θ and φ. Inserting these formulas into (41), we obtain, after some simplifications, an equation of the form $F(k^2, a_0, a_2, \ldots) = 0$, where F is a polynomial function. In order to calculate recursively the unknown coeficients a_0, a_2, etc., we impose that the successive derivatives of the F function (in k^2) at the origin vanish. For simplicity, we will admit in the remainder of this section that $k_3 = 0$, i.e., the modes propagate in the $x_3 = 0$ plane.

Using the approach delineated above, we verified that there exist five modes in the long wavelength limit. The dispersion characteristic of the modes is

$$\beta^2 = 0 + o(k^6)$$
$$k_3 = 0 \tag{44a}$$
$$\beta^2 = \frac{2k_1^2 k_2^2}{\beta_0^2} + o(k^6)$$
$$k_3 = 0 \tag{44b}$$
$$\beta^2 = \beta_0^2 + k^2 \pm k_1 k_2 + o(k^4)$$
$$k_3 = 0 \tag{44c}$$
$$\beta^2 = \beta_0^2 + k^2 + o(k^4)$$
$$k_3 = 0. \tag{44d}$$

In the above, $o(t)$ represents an expression that vanishes at the same rate as t. Equation (44c) represents the dispersion characteristic of two different modes: one associated with the "+" sign and the other one with the "−" sign. The polarization of the modes can be calculated using [18, p. 202 (with a different notation)]

$$\mathbf{E}_{\text{av}} \propto \left(\frac{k_x}{k^2 - \beta^2 \varepsilon_{xx}}, \frac{k_y}{k^2 - \beta^2 \varepsilon_{yy}}, \frac{k_z}{k^2 - \beta^2 \varepsilon_{zz}} \right). \tag{45}$$

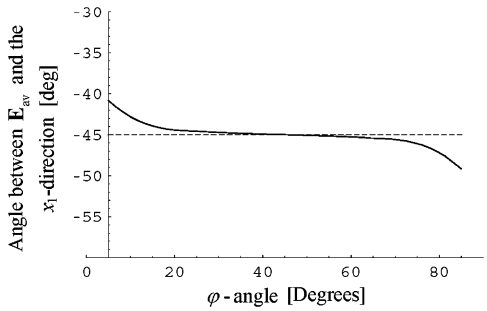

Fig. 6. Angle between the electric field and the x_1-axis for the "+" mode defined by (44c) (full line: numerical results; dashed line: theory).

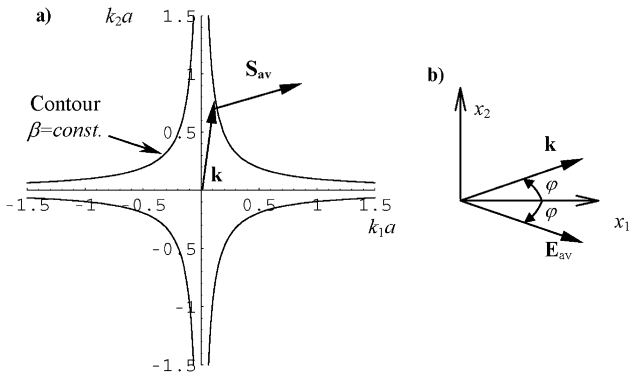

Fig. 7. (a) Generic wave normal contour of the mode defined by (44b). (b) Theoretical geometrical relation between the associated average electric field and wave vector.

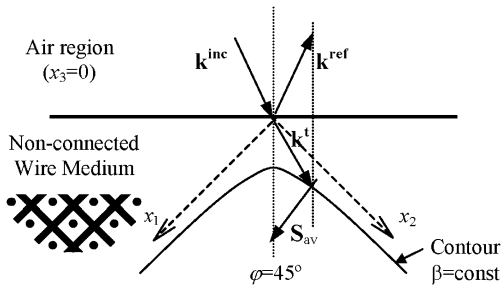

Fig. 8. Negative refraction occurs at an interface between air and the non-connected wire medium (the inset shows the orientation of the metamaterial).

The modes defined by (44c) and (44d) were discussed in [8]. For completeness, we will briefly review their main properties.

The mode defined by (44d) is a TEM mode with polarization along the x_3-direction (i.e., normal to the plane of propagation). On the other hand, the two modes defined by (44c) have elliptic wave normal contours (the principal axes are defined by $\varphi = \pm 45°$). The polarization of these modes is on the $x_3 = 0$ plane and, to a first-order approximation, is independent of the wave vector $\mathbf{E}_{\rm av} \propto (1, -(\pm 1), 0)$. This result is the leading term of the formula that is obtained by substituting (44c) into (45).

In Fig. 6, we compare the formula for the electric field with full-wave numerical simulations obtained using the method proposed in [8] (we computed the electromagnetic modes, and then we averaged the fields over the unit cell to calculate the polarization of the field). The wire radius is $r_w = 0.01a$. We put $\mathbf{k} = k(\cos\varphi, \sin\varphi, 0)$, where $k = 0.07\pi/a$, and we computed the angle that the average electric field associated with the "+" mode makes with the x_1-axis as a function of φ. We compared the result with the expected value $\varphi = -45°$. As seen in Fig. 6, the agreement is good, especially for directions not too close to the axes. The discrepancy along the wire axes is not relevant because the modes defined by (44c) are degenerate along those directions.

The described results show that the propagation in the non-connected wire medium is very different from the propagation in the connected wire medium. Indeed, the modes that propagate in the two materials have distinct polarizations and dispersion characteristics. The nonconnected medium does not support TEM waves and, thus, it is not suitable for applications in which the metamaterial is supposed to mimic the properties of ideal cold plasma.

In what follows, we discuss the properties of the electromagnetic modes corresponding to (44a) and (44b). The mode associated with (44a) is longitudinal and nearly dispersionless (for $k_3 = 0$). Thus, it is not relevant for propagation on the $x_3 = 0$ plane. On the other hand, the mode associated with (44b) has a remarkable feature: the wave normal contours $\beta = \text{const}$ are hyperbolic near the static limit. This situation is rather peculiar and does not occur in standard (nonartificial) dielectric materials, which invariably have elliptic wave normal surfaces. In Fig. 7(a), we plot a generic $\beta = \text{const}$ contour. We also depict a generic wave vector $\mathbf{k}$ and the corresponding Poynting vector $\mathbf{S}_{\rm av}$. As is well known, the Poynting vector is perpendicular to the wave normal surface [14, p. 95].

For $k_3 = 0$, the polarization is to a first approximation $\mathbf{E}_{\rm av} \propto (k_1, -k_2, 0)$. This expression is the leading term of the formula that is obtained by inserting (44b) into (45). In particular, if the wave vector is along a coordinate axis, the mode is longitudinal. The geometrical relation between the wave vector and electric field is depicted in Fig. 7(b). The electric field and wave vector make the same angle with the coordinates axes.

To our best knowledge, no one has ever reported an artificial material with similar properties near the static limit. This mode propagates only at very large wavelengths before it enters in cutoff. The interesting thing is that the hyperbolic contours originate negative refraction at an interface with air. Indeed, since the component of $\mathbf{k}$ parallel to the interface is preserved and the rays are parallel to the Poynting vector, we have the ray picture illustrated in Fig. 8. Note that we have negative refraction, but not a backward wave.

In Fig. 8, the vector $\mathbf{k}^{\rm inc}$ represents the wave vector of the ray that impinges on the interface, $\mathbf{k}^{\rm ref}$ is the wave vector associated with the reflected ray, and $\mathbf{k}^t$ is the wave vector associated with the transmitted ray. We also depicted the $\beta = \text{const}$ contour. The transmitted wave vector lies on the $\beta = \text{const}$ contour and its projection onto the interface is equal to the projection of $\mathbf{k}^{\rm inc}$ and $\mathbf{k}^{\rm ref}$ onto the interface. The transmitted ray propagates along the direction of the Poynting vector $\mathbf{S}_{\rm av}$. It is clear from Fig. 8 that the negative refraction phenomenon occurs. Note that the interface with air is normal to the direction $\varphi = 45°$, where φ is measured relatively to the x_1-axis (as usual, the wires are directed along the coordinate axes).

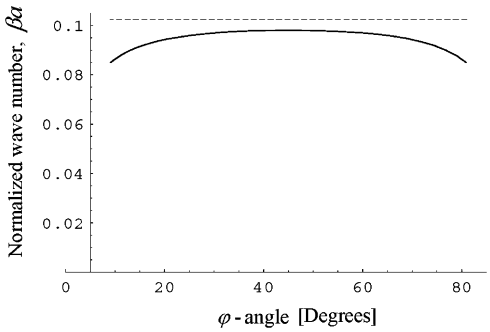

Fig. 9. Calculated β (full line) and theoretical β (dashed line) along a hyperbolic contour in the k-plane (i.e., as a function of the φ-angle).

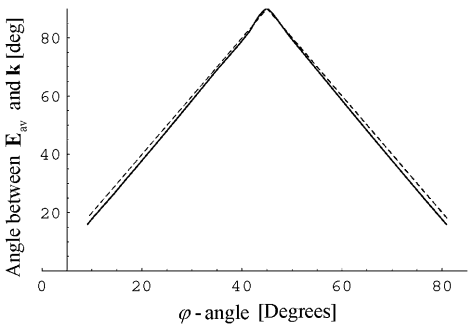

Fig. 10. Angle between the electric field and wave vector as a function of the φ-angle (mode with hyperbolic contour; full line: numerical results; dashed line: theory).

In Fig. 9, the theoretical dispersion characteristic of the mode (44b) is compared with full-wave numerical results obtained using the method proposed in [8]. We put $\mathbf{k} = k(\varphi)(\cos\varphi, \sin\varphi, 0)$, where $k(\varphi)$ is calculated in order that the wave vector satisfies (44b) for $\beta a = 0.1$ (the free-space wavelength is $\lambda = 62.8a$). We then computed β numerically as a function of φ, and we compared it with the theoretical value (i.e., $\beta a = 0.1$). As seen in Fig. 9, the computed value compares well with the theoretical value, and is practically constant (even near the coordinate axes where the long wavelength limit approximation fails; indeed the condition $|\mathbf{k}|a \ll 2\pi$ is not fulfilled for $\beta = \text{const}$).

In addition, we calculated the polarization of the electromagnetic mode numerically and we compared it with the formula $\mathbf{E}_{\text{av}} \propto (k_1, -k_2, 0)$. As before, we put $\mathbf{k} = k(\varphi)(\cos\varphi, \sin\varphi, 0)$, and we computed the angle between the average electric field and wave vector as a function of φ. The result is depicted in Fig. 10. The agreement between the analytical model and simulations is excellent.

VII. Conclusions

In this paper, we discussed the electrodynamics of the 3-D-wire medium in the long wavelength limit. We considered two distinct topologies for the wire inclusions: the connected topology and nonconnected topology. We found that the properties of the effective medium are surprisingly dependent on the topology of the metamaterial. Based on simple physical considerations and using an integral-equation-based formulation, we were able to reduce the modal problem to the calculation of the zeros of the determinant of a characteristic system known in closed analytical form. We have proven that the permittivity dyadic can be extracted unambiguously from the characteristic system. We obtained an analytic model for the permittivity dyadic of the wire medium. The permittivity dyadic depends on the wave vector and, thus, there is always spatial dispersion.

However, we found that the connected wire medium supports two TEM degenerate waves. These waves propagate as in an ideal isotropic medium with negative permittivity. Therefore, as discussed in the text, this topology of the wire medium is a good candidate for many relevant metamaterial applications (e.g., DNG materials).

On the other hand, in the nonconnected medium, the waves are, in general, neither TEM, nor degenerate. Moreover, near the plasma frequency, the polarization of the fields is almost independent of the wave vector. Thus, we conclude that this topology of the wire medium is not appropriate for metamaterial applications in which the material must supposedly mimic the properties of an ideal plasma. Our results also show that, near the static limit, the dispersion characteristic of the modes is intrinsically hyperbolic. This result is remarkable because the materials usually available in nature have elliptic wave normal surfaces. A consequence of this unusual property is that negative refraction may occur at an interface between air and the nonconnected wire medium.

Appendix A

Here, we calculate the dyadics defined by (25) and (26). To begin, we note that, in the long wavelength limit (16), we can replace the term $1/(\mathbf{k_J} \cdot \mathbf{k_J} - \beta^2)$ by $1/|\mathbf{k_J^0}|^2$ in the spectral representation of the Green function (8), except in the parcel associated with the index $\mathbf{J} = \mathbf{0}$. We obtain the approximate formula

$$\mathbf{\Phi}_p(\mathbf{r}|\mathbf{r}') \approx \frac{1}{V_{\text{cell}}} \frac{e^{-j\mathbf{k}\cdot(\mathbf{r}-\mathbf{r}')}}{k^2 - \beta^2} + \frac{1}{V_{\text{cell}}} \sum_{\mathbf{J}\neq\mathbf{0}} \frac{e^{-j\mathbf{k_J}\cdot(\mathbf{r}-\mathbf{r}')}}{|\mathbf{k_J^0}|^2} \quad \text{(A1)}$$

where $\mathbf{J} = (j_1, j_2, j_3)$ is a multiindex of integers and $\mathbf{K_J^0} = (2\pi/a)\mathbf{J}$. In the following, we evaluate the desired dyadics using always the above approximation for the Green function.

A. Connected Topology

Here, we assume that the topology of the wire medium is connected. We first calculate the dyadic $\overline{\overline{\mathbf{A}_{\text{I}}}}$ defined by (25b). Inserting (19) into (15b), we easily obtain

$$\hat{\mathbf{u}}_p \cdot \overline{\overline{\mathbf{A}_{\text{I}}}} \cdot \hat{\mathbf{u}}_q = \chi\left(\mathbf{w}_p^{\text{I}}, \mathbf{w}_q^{\text{I}}\right) = \left(k_p k_q - \beta^2 \delta_{p,q}\right) g_{p,q}^{(1)} \quad \text{(A2)}$$

where $g_{p,q}^{(1)}$ is defined by (B1). Using (B4) and the identity $\overline{\overline{\mathbf{A}_{\text{I}}}} = \sum_{p,q} \hat{\mathbf{u}}_p \hat{\mathbf{u}}_p \cdot \overline{\overline{\mathbf{A}_{\text{I}}}} \cdot \hat{\mathbf{u}}_q \hat{\mathbf{u}}_q$, we find that

$$\overline{\overline{\mathbf{A}_{\text{I}}}} = \frac{1}{V_{\text{cell}}} \left(\frac{1}{k^2 - \beta^2} + \frac{1}{\beta_1^2} \right) \left(\mathbf{kk} - \beta^2 \overline{\overline{\mathbf{I}}} \right) + \frac{1}{V_{\text{cell}}} \left(\frac{1}{\beta_0^2} - \frac{1}{\beta_1^2} \right) \sum_{1 \le p \le 3} \left(k_p^2 - \beta^2 \right) \hat{\mathbf{u}}_p \hat{\mathbf{u}}_p \quad \text{(A3)}$$

where $\overline{\overline{\mathbf{I}}}$ is the identity dyadic. The constants β_0 and β_1 are defined in Appendix B.

We now calculate the dyadic $\overline{\overline{\mathbf{L}}}$ defined by (25d). Inserting (19) and (20) into (15b), we obtain

$$\begin{aligned}\hat{\mathbf{u}}_p \cdot \overline{\overline{\mathbf{L}}} \cdot \hat{\mathbf{u}}_q &= \chi\left(\mathbf{w}_p^{\mathrm{I}}, \mathbf{w}_q^{\mathrm{II}}\right) \\ &= \sum_n \left(\left(k_p k_n - \beta^2 \delta_{p,n}\right) \alpha_{q,n} g_{p,n}^{(2)} - \frac{jk_p}{a} \alpha_{q,n} g_{p,n}^{(1)} \right).\end{aligned} \tag{A4}$$

The coefficient $g_{m,n}^{(2)}$ is defined by (B1b) and, as proven in Appendix B, is identically zero. Using (B4) and the continuity equation $\sum_n \alpha_{q,n} = 0$, we find that

$$\hat{\mathbf{u}}_p \cdot \overline{\overline{\mathbf{L}}} \cdot \hat{\mathbf{u}}_q = -\frac{1}{V_{\mathrm{cell}}} \left(\frac{1}{\beta_0^2} - \frac{1}{\beta_1^2} \right) \frac{jk_p}{a} \alpha_{q,p}. \tag{A5}$$

Therefore, we have

$$\overline{\overline{\mathbf{L}}} = \frac{1}{V_{\mathrm{cell}}} \frac{1}{ja} \left(\frac{1}{\beta_0^2} - \frac{1}{\beta_1^2} \right) \left(\sum_{1 \le p \le 3} k_p \hat{\mathbf{u}}_p \hat{\mathbf{u}}_p \right) \left(\sum_{1 \le q \le 2} \alpha_q \hat{\mathbf{u}}_q \right). \tag{A6}$$

The dyadic $\overline{\overline{\mathbf{L}^*}}$ is given by

$$\begin{aligned}\overline{\overline{\mathbf{L}^*}} = -\frac{1}{V_{\mathrm{cell}}} \frac{1}{ja} \left(\frac{1}{\beta_0^2} - \frac{1}{\beta_1^2} \right) &\left(\sum_{1 \le q \le 2} \hat{\mathbf{u}}_q \alpha_q \right) \\ &\cdot \left(\sum_{1 \le p \le 3} k_p \hat{\mathbf{u}}_p \hat{\mathbf{u}}_p \right).\end{aligned} \tag{A7}$$

We next calculate the dyadic $\overline{\overline{\mathbf{A}_{\mathrm{II}}}}$ defined by (25c). Inserting (20) into (15b), we obtain

$$\begin{aligned}\hat{\mathbf{u}}_p \cdot \overline{\overline{\mathbf{A}_{\mathrm{II}}}} \cdot \hat{\mathbf{u}}_q &= \chi\left(\mathbf{w}_p^{\mathrm{II}}, \mathbf{w}_q^{\mathrm{II}}\right) \\ &= \sum_{m,n} (k_m k_n - \beta^2 \delta_{m,n}) \alpha_{p,m} \alpha_{q,n} g_{m,n}^{(3)} \\ &\quad + \sum_{m,n} \frac{1}{a^2} \alpha_{p,m} \alpha_{q,n} g_{m,n}^{(1)} \\ &\quad + \sum_{m,n} \frac{jk_n}{a} \alpha_{p,m} \alpha_{q,n} g_{m,n}^{(2)} \\ &\quad + \sum_{m,n} \frac{-jk_m}{a} \alpha_{p,m} \alpha_{q,n} (g_{n,m}^{(2)})^*.\end{aligned} \tag{A8}$$

In the above, the $g_{m,n}$ coefficients are defined by (B1). Using (B4), (B8), (B10), and the continuity condition, we obtain

$$\begin{aligned}\hat{\mathbf{u}}_p \cdot \overline{\overline{\mathbf{A}_{\mathrm{II}}}} \cdot \hat{\mathbf{u}}_q = &\frac{1}{V_{\mathrm{cell}}} \frac{1}{\beta_2^2} \sum_m \left(k_m^2 - \beta^2\right) \alpha_{p,m} \alpha_{q,m} \\ &+ \frac{1}{V_{\mathrm{cell}}} \left(\frac{1}{\beta_0^2} - \frac{1}{\beta_1^2} \right) \frac{1}{a^2} \sum_m \alpha_{p,m} \alpha_{q,m}.\end{aligned} \tag{A9}$$

The constant β_2 is defined by (B10b). In the long wavelength limit, the first term on the right-hand side can be neglected. Indeed, if we would decide to keep that term, we would find that the correction in the final result would be comparable with the error introduced by the approximation (A1). Hence, using (22), we conclude that

$$\overline{\overline{\mathbf{A}}}_{\mathrm{II}} \approx \frac{1}{V_{\mathrm{cell}}} \left(\frac{1}{\beta_0^2} - \frac{1}{\beta_1^2} \right) \frac{1}{a^2} \sum_{1 \le p \le 2} \hat{\mathbf{u}}_p \hat{\mathbf{u}}_p. \tag{A10}$$

We are now ready to calculate the dyadic $\overline{\overline{\mathbf{A}}}$ defined by (26). Straightforward calculations show that

$$\begin{aligned}\overline{\overline{\mathbf{L}}} \cdot \overline{\overline{\mathbf{A}_{\mathrm{II}}}}^{-1} \cdot \overline{\overline{\mathbf{L}^*}} = \frac{1}{V_{\mathrm{cell}}} \left(\frac{1}{\beta_0^2} - \frac{1}{\beta_1^2} \right) &\times \left(\sum_{1 \le p \le 3} k_p \hat{\mathbf{u}}_p \hat{\mathbf{u}}_p \right) \\ &\cdot \left(\sum_{1 \le q \le 3} \alpha_q \alpha_q \right) \cdot \left(\sum_{1 \le p \le 3} k_p \hat{\mathbf{u}}_p \hat{\mathbf{u}}_p \right).\end{aligned} \tag{A11}$$

We note that (22) implies that

$$\overline{\overline{\mathbf{I}}} = \left(\sum_{1 \le q \le 3} \hat{\mathbf{u}}_q \alpha_q \right) \cdot \left(\sum_{1 \le q \le 3} \alpha_q \hat{\mathbf{u}}_q \right). \tag{A12}$$

However, we then necessarily have

$$\overline{\overline{\mathbf{I}}} = \left(\sum_{1 \le q \le 3} \alpha_q \hat{\mathbf{u}}_q \right) \cdot \left(\sum_{1 \le q \le 3} \hat{\mathbf{u}}_q \alpha_q \right) = \sum_{1 \le q \le 3} \alpha_q \alpha_q \tag{A13}$$

and, in particular, we find that

$$\sum_{1 \le q \le 2} \alpha_q \alpha_q = \overline{\overline{\mathbf{I}}} - \alpha_3 \alpha_3. \tag{A14}$$

Inserting the above result into (A11) and using (21), we obtain

$$\begin{aligned}\overline{\overline{\mathbf{L}}} \cdot \overline{\overline{\mathbf{A}_{\mathrm{II}}}}^{-1} \cdot \overline{\overline{\mathbf{L}^*}} = \frac{1}{V_{\mathrm{cell}}} &\left(\frac{1}{\beta_0^2} - \frac{1}{\beta_1^2} \right) \\ &\cdot \left(\sum_{1 \le p \le 3} k_p^2 \hat{\mathbf{u}}_p \hat{\mathbf{u}}_p - \frac{1}{3} kk \right).\end{aligned} \tag{A15}$$

Substituting the previous formula and (A3) into (26), we obtain (27).

B. Nonconnected Topology

Here, we calculate the dyadic $\overline{\overline{\mathbf{A}}}$ for the case in which the topology of the wire medium is nonconnected. From (26), we have $\overline{\overline{\mathbf{A}}} = \overline{\overline{\mathbf{A}_{\mathrm{I}}}}$. Since the results of the above section remain valid, the dyadic $\overline{\overline{\mathbf{A}_{\mathrm{I}}}}$ is still given by (A3). However, we note that the dyadic is not the same in the two cases because the constant β_1^2 depends on the topology of the wire medium [see(B6)]. We also note that $1/\beta_0^2 \gg 1/\beta_1^2$ because $1/\beta_1^2$ is given by an oscillating series, whereas $1/\beta_0^2$ is given by a double nonoscillating

series. Therefore, in the long wavelength limit, we can clearly neglect the term $1/\beta_1^2$ in (A3). This approximation yields (27).

APPENDIX B

Here, we calculate the following auxiliary integrals assuming that (A1) holds exactly:

$$g_{m,n}^{(1)} = \frac{1}{a^2(2\pi r_w)^2}\int_{\partial D_m} ds \int_{\partial D_n} ds' \Phi_p(\mathbf{r}|\mathbf{r}') \cdot e^{j\mathbf{k}\cdot(\mathbf{r}-\mathbf{r}')} \tag{B1a}$$

$$g_{m,n}^{(2)} = \frac{1}{a^2(2\pi r_w)^2}\int_{\partial D_m} ds \int_{\partial D_n} ds' s(x_n') \Phi_p(\mathbf{r}|\mathbf{r}') \cdot e^{j\mathbf{k}\cdot(\mathbf{r}-\mathbf{r}')} \tag{B1b}$$

$$g_{m,n}^{(3)} = \frac{1}{a^2(2\pi r_w)^2}\int_{\partial D_m} ds \int_{\partial D_n} ds' s(x_m) s(x_n') \cdot \Phi_p(\mathbf{r}|\mathbf{r}') e^{j\mathbf{k}\cdot(\mathbf{r}-\mathbf{r}')}. \tag{B1c}$$

Using (A1), we easily find that $g_{m,n}^{(1)}$ is equal to

$$g_{m,n}^{(1)} = \frac{1}{V_{\text{cell}}}\left(\frac{1}{k^2-\beta^2} + \frac{1}{\beta_{m,n}^2}\right) \tag{B2}$$

where $\beta_{m,n}^2$ is the constant (independent of β and $\mathbf{k}$) defined by

$$\frac{1}{\beta_{m,n}^2} = \sum_{\mathbf{J}\neq\mathbf{0}} \frac{1}{|\mathbf{k}_\mathbf{J}^\mathbf{0}|^2} \vartheta_{\mathbf{J},m}\vartheta_{\mathbf{J},n}^* = \sum_{\substack{\mathbf{J}\neq\mathbf{0}\\ j_m=j_n=0}} \frac{\left[J_0\left(|\mathbf{k}_\mathbf{J}^\mathbf{0}| r_w\right)\right]^2}{|\mathbf{k}_\mathbf{J}^\mathbf{0}|^2} e^{-j\mathbf{k}_\mathbf{J}^\mathbf{0}\cdot(\mathbf{r}_{0,m}-\mathbf{r}_{0,n})} \tag{B3a}$$

$$\vartheta_{\mathbf{J},m} = \frac{1}{a(2\pi r_w)}\int_{\partial D_m} e^{-j\mathbf{k}_\mathbf{J}^\mathbf{0}\cdot r} ds = \delta_{j_m,0} J_0\left(|\mathbf{k}_\mathbf{J}^\mathbf{0}| r_w\right) e^{-j\mathbf{k}_\mathbf{J}^\mathbf{0}\cdot\mathbf{r}_{0,m}}. \tag{B3b}$$

In the above, J_0 stands for the Bessel function of the first kind and order 0, and $\mathbf{r}_{0,n}$ is the center of the wire directed in the x_n-direction. For the connected topology, we have $\mathbf{r}_{0,n} = \mathbf{0}$, while for the nonconnected topology, $\mathbf{r}_{0,n}$ is given by (4). We note that $\beta_{m,n}^2$ has only two different values, more specifically, $\beta_{m,n}^2 = \beta_0^2$ if $m = n$ and $\beta_{m,n}^2 = \beta_1^2$ if $m \neq n$. Therefore, we can rewrite (B2) as follows:

$$g_{m,n}^{(1)} = \frac{1}{V_{\text{cell}}}\left(\frac{1}{k^2-\beta^2} + \frac{1}{\beta_1^2} + \left(\frac{1}{\beta_0^2} - \frac{1}{\beta_1^2}\right)\delta_{m,n}\right). \tag{B4}$$

The constant β_0^2 is independent of the wire medium being connected or not, and is always positive. It is defined by

$$\frac{1}{\beta_0^2} = \left(\frac{a}{2\pi}\right)^2 \sum_{(l,r)\neq(0,0)} \frac{\left[J_0\left(\sqrt{l^2+r^2}\frac{2\pi r_w}{a}\right)\right]^2}{l^2+r^2} \tag{B5}$$

where l and r are integers. On the other hand, the constant β_1^2 depends on the topology of the wire medium, and can be negative. It can be written as

$$\frac{1}{\beta_1^2} = \left(\frac{a}{2\pi}\right)^2 \sum_{l\neq 0} \frac{\left[J_0\left(\frac{2\pi l r_w}{a}\right)\right]^2}{l^2} \times \begin{cases} 1 & \text{connected topology} \\ (-1)^l & \text{nonconnected topology} \end{cases} \tag{B6}$$

where l is an integer different from zero.

In the remainder of this Appendix, we will always assume that the wires are connected. Next, we calculate $g_{m,n}^{(2)}$. We obtain

$$g_{m,n}^{(2)} = \frac{1}{V_{\text{cell}}}\sum_{\mathbf{J}\neq\mathbf{0}} \frac{1}{|\mathbf{k}_\mathbf{J}^\mathbf{0}|^2}\vartheta_{\mathbf{J},m}\varsigma_{\mathbf{J},n}^* = \frac{1}{V_{\text{cell}}}\sum_{\substack{\mathbf{J}\neq\mathbf{0},\\ j_m=0}} \frac{1}{|\mathbf{k}_\mathbf{J}^\mathbf{0}|^2} J_0\left(|\mathbf{k}_\mathbf{J}^\mathbf{0}| r_w\right)\varsigma_{\mathbf{J},n}^* \tag{B7a}$$

$$\varsigma_{\mathbf{J},m} = \frac{1}{a(2\pi r_w)}\int_{\partial D_m} e^{-j\mathbf{k}_\mathbf{J}^\mathbf{0}\cdot\mathbf{r}} s(x_m) ds = J_0\left(\sqrt{|\mathbf{k}_\mathbf{J}^\mathbf{0}|^2 - \left(\frac{2\pi j_m}{a}\right)^2} r_w\right)\frac{1}{a} \cdot \int_{-a/2}^{a/2} s(x) e^{-j((2\pi)/a)j_m x} dx. \tag{B7b}$$

Taking into account the symmetries of the summation range in the index j_n and the fact of the "saw" function being odd, it is easy to verify that

$$g_{m,n}^{(2)} = 0. \tag{B8}$$

Finally, we calculate $g_{m,n}^{(3)}$. We have

$$g_{m,n}^{(3)} = \frac{1}{V_{\text{cell}}}\sum_{\mathbf{J}\neq\mathbf{0}} \frac{1}{|\mathbf{k}_\mathbf{J}^\mathbf{0}|^2}\varsigma_{\mathbf{J},m}\varsigma_{\mathbf{J},n}^*. \tag{B9}$$

If $m \neq n$, the series vanishes for reasons similar to those discussed during the calculation of $g_{m,n}^{(2)}$. Therefore, we have

$$g_{m,n}^{(3)} = \delta_{m,n}\frac{1}{V_{\text{cell}}}\frac{1}{\beta_2^2} \tag{B10a}$$

$$\frac{1}{\beta_2^2} = \sum_{\mathbf{J}\neq\mathbf{0}} \frac{1}{|\mathbf{k}_\mathbf{J}^\mathbf{0}|^2}\left[J_0\left(\sqrt{|\mathbf{k}_\mathbf{J}^\mathbf{0}|^2 - \left(\frac{2\pi j_m}{a}\right)^2} r_w\right)\right]^2 \cdot \left|\frac{1}{a}\int_{-a/2}^{a/2} s(x) e^{-j((2\pi)/a)j_m x} dx\right|^2. \tag{B10b}$$

Note that the definition of β_2^2 is independent of the m index, and that β_2^2 is a constant.

APPENDIX C

Here, we generalize without proof the results of the paper to the 2-D-wire medium. In this metamaterial, the wires are oriented exclusively along the x_1- and x_2- directions. In the case of the nonconnected topology, the permittivity dyadic is given

by (39b), except that the m index is restricted to $m = 1, 2$. On the other hand, in case of the connected topology, the permittivity dyadic is given by (39a) with the symbol $\mathbf{k}$ replaced by $\mathbf{k}_{||} = k_1\hat{\mathbf{u}}_1 + k_2\hat{\mathbf{u}}_2$, and the $\bar{\bar{\mathbf{I}}}$ dyadic inside brackets replaced by $\bar{\bar{\mathbf{I}}}_{||} = \hat{\mathbf{u}}_1\hat{\mathbf{u}}_1 + \hat{\mathbf{u}}_2\hat{\mathbf{u}}_2$. The constant l_0 is defined as shown in (39a) with the symbol "3" replaced by "2."

REFERENCES

[1] D. R. Smith, W. J. Padilla, D. C. Vier, S. C. Nemat-Nasser, and S. Schultz, "Composite medium with simultaneously negative permeability and permittivity," *Phys. Rev. Lett.*, vol. 84, pp. 4184–4187, May 2000.

[2] R. A. Shelby, D. R. Smith, and S. Schultz, "Experimental verification of a negative index of refraction," *Science*, vol. 292, pp. 77–79, Apr. 2001.

[3] D. R. Smith, S. Schultz, P. Markos, and C. M. Soukoulis, "Determination of effective permittivity and permeability of metamaterials from reflection and transmission coefficients," *Phys. Rev. B, Condens. Matter*, vol. 65, pp. 195 1041–195 104 5, Apr. 2002.

[4] V. G. Veselago, "Electrodynamics of substances with simultaneously negative electrical and magnetic permeabilities," *Sov. Phys.—Usp.*, vol. 10, pp. 509–514, Jan.–Feb. 1968.

[5] G. V. Eleftheriades, A. K. Iyer, and P. C. Kremer, "Planar negative refractive index media using periodically *L–C* loaded transmission lines," *IEEE Trans. Microw. Theory Tech.*, vol. 50, no. 12, pp. 2702–2712, Dec. 2002.

[6] J. B. Pendry, "Negative refraction makes a perfect lens," *Phys. Rev. Lett.*, vol. 85, no. 18, pp. 3966–3969, Oct. 2000.

[7] N. Engheta, "An idea for thin, subwavelength cavity resonators using metamaterials with negative permittivity and permeability," *IEEE Antennas Wireless Propag. Lett.*, vol. 1, no. Dec., pp. 10–13, 2002.

[8] M. Silveirinha and C. A. Fernandes, "A hybrid method for the efficient calculation of the band structure of 3-D-metallic crystals," *IEEE Trans. Microw. Theory Tech.*, no. 3, pp. 889–902, Mar. 2004.

[9] P. A. Belov, R. Marqués, S. I. Maslovski, I. S. Nefedov, M. Silveirinha, C. R. Simovski, and S. A. Tretyakov, "Strong spatial dispersion in wire media in the very large wavelength limit," *Phys. Rev. B, Condens. Matter*, vol. 67, pp. 113 1031–113 1034, 2003.

[10] C. A. Moses and N. Engheta, "Electromagnetic wave propagation in the wire medium: A complex medium with long thin inclusions," *Wave Motion*, vol. 34, pp. 301–317, 2001.

[11] A. Alu and N. Engheta, "Pairing an epsilon-negative slab with a mu-negative slab: Resonance, tunneling and transparency," *IEEE Trans. Antennas Propag.*, vol. 51, no. 10, pp. 2558–2571, Oct. 2003.

[12] D. F. Sievenpiper, M. E. Sickmiller, and E. Yablanovitch, "3D wire mesh photonic crystals," *Phys. Rev. Lett.*, vol. 76, pp. 2480–2483, 1996.

[13] E. Sayre, "Junction discontinuities in wire antenna and scattering problems," *IEEE Trans. Antennas Propag.*, vol. 21, no. 2, pp. 216–217, Mar. 1973.

[14] K. Sakoda, *Optical Properties of Photonic Crystals*, ser. Opt. Sci.. Berlin, Germany: Springer-Verlag, 2001, vol. 80.

[15] P. P. Ewald, "Die berechnung optischer und elektrostatischer gitterpotentiale," *Ann. Phys. (Germany)*, vol. 64, pp. 253–287, 1921.

[16] M. Silveirinha and C. A. Fernandes, "A new acceleration technique with exponential convergence rate to evaluate periodic Green's functions," *IEEE Trans. Antennas Propag.*, vol. 53, no. 1, pp. 347–355, Jan. 2005.

[17] M. Silveirinha, "Electromagnetic waves in artificial media with application to lens antennas," Ph.D. dissertation, Dept. Elect. Comput. Eng., Univ. Técnica de Lisboa, Lisbon, Portugal, 2003.

[18] R. E. Collin, *Field Theory of Guided Waves*, 2nd ed. New York: IEEE Press, 1991.

[19] C. Dougherty, *Electrodynamics of Particles and Plasmas*. Reading, MA: Addison-Wesley, 1969, pp. 175–178.

[20] S. I. Maslovski and S. A. Tretyakov, "Additional boundary conditions for spatially dispersive media," in *Proc. 8th Bianisotropics Conf.*, Lisbon, Portugal, Sep. 2000, pp. 7–10.

[21] W. A. Davis and C. M. Krowne, "The effects of drift and diffusion in semiconductors on plane wave interaction at interfaces," *IEEE Trans. Antennas Propag.*, vol. 36, no. 1, pp. 97–103, Jan. 1998.

[22] J. B. Pendry, A. J. Holden, D. J. Robins, and W. J. Stewart, "Magnetism from conductors and enhanced nonlinear phenomena," *IEEE Trans. Microw. Theory Tech.*, vol. 47, no. 11, pp. 2075–2084, Nov. 1999.

[23] C. R. Simovski and P. A. Belov, "Low-frequency spatial dispersion in wire media," *Phys. Rev. E, Stat. Phys. Plasmas Fluids Relat. Interdiscip. Top.*, vol. 70, p. 046 616, Oct. 2004.

Mário G. Silveirinha (S'99–M'03) received the Licenciado degree in electrical engineering from the University of Coimbra, Coimbra, Portugal, in 1998, and the Ph.D. degree in electrical and computer engineering from the Instituto Superior Técnico (IST), Technical University of Lisbon, Lisbon, Portugal, in 2003.

His research interests include propagation in photonic crystals and homogenization and modeling of metamaterials.

Carlos A. Fernandes (S'86–M'89) received the Licenciado, M.Sc., and Ph.D. degrees in electrical and computer engineering from the Instituto Superior Técnico (IST), Technical University of Lisbon, Lisbon, Portugal, in 1980, 1985, and 1990, respectively.

In 1980, he joined the IST, where, since 1993, he has been an Associate Professor with the Department of Electrical and Computer Engineering. He is involved in the areas of microwaves, radio-wave propagation, and antennas. Since 1993, he has been a Senior Researcher with the Instituto de Telecomunicações, where he is currently the Coordinator of the wireless communications scientific area. He coauthored a book, a book chapter, and several technical papers in international journals and conference proceedings in the areas of antennas and radio-wave propagation modeling. His current research interests include artificial dielectrics, dielectric antennas for millimeter-wave applications, and propagation modeling for mobile communication systems.

Dr. Fernandes has been the leader of antenna activity with National and European Projects such as RACE 2067—Mobile Broadband System (MBS) and ACTS AC230—System for Advanced Mobile Broadband Applications (SAMBA).